FTD-ID(RS)T-0571-91

FOREIGN TECHNOLOGY DIVISION

STUDIES ON THE COMBUSTION EFFICIENCY OF LIQUID FUEL ROCKETS WITH VARIABLE THRUST

by

Li Xiaobin, Chen Qizhi, Chen Yunqin

HUMAN TRANSLATION

FTD-ID(RS)T-0571-91 3 December 1991

STUDIES ON THE COMBUSTION EFFICIENCY OF LIQUID FUEL ROCKETS WITH VARIABLE THRUST

By: Li Xiaobin, Chen Qizhi, Chen Yunqin

English pages: 25

Source: Yuhang Xuebao, Nr. 3, 1986, pp. 61-72

Country of origin: China
Translated by: SCITRAN
F33657-84-D-0165
Requester: FTD/TTTAV/A.G. Crowder

PREPARED BY:

TRANSLATION DIVISION
FOREIGN TECHNOLOGY DIVISION
WPAFB, OHIO

GRAPHICS DISCLAIMER

All figures, graphics, tables, equations, etc. merged into this translation were extracted from the best quality copy available.

TITLE: STUDIES ON THE COMBUSTION EFFICIENCY OF LIQUID FUEL ROCKETS WITH VARIABLE THRUST

AUTHOR: Li Xiaobin, Chen Qizhi, Chen Yunqin

SUMMARY

This article carries out studies on the stability characteristics of liquid fuel rocket engines within a relatively large range of variations. The research work was carried out centering around the speed and efficiency characteristics of combustion chambers. This article sets out the results of relevent experiments and theoretical calculations. From the angle of the combustion processes within combustion chambers, there were clear indications of the status of the effects of various processes (for example, evaporation or vaporization, mixing, chemical reactions, etc.) following along with changes in the operatinal status of variable thrust engine combustion efficiency.

SYMBOL EXPLANATIONS

A_c combustion chamber cross section area cm^2; $\dot{m}$ propellant mass flow kg/s; A_t jet tube throat area cm^2; $\dot{m}_{vap}$ liquid drop evaporation rate kg/s; C_p constant pressure specific heat $J/kg \cdot {}^oK$; N liquid drop number in unit volume $1/cm^3$; C^* characteristic speed m/s; p pressure N/m^2; D diffussion coefficient m^2/s; Q heat added to liquid drop in unit time by gases J/s; E decomposition reaction activation energy J/kgmol; $\vec{F}$ effective or applied force of gases on liquid drop kg; Q_c decomposition reaction heat J/kg; $\vec{g}$ strength of flow kg/s m^2; $\vec{q}$ heat flow strength vector $J/s \cdot m^2$; g_B initial propellant evaporization or vaporization fraction ; g_e heat liquid drop heat exchange rate J/s; H total liquid drop unit mass enthalpy J/kg; R universal gas constant $J/kg \cdot {}^oK$; h degree of opening of jet injector needle valves mm; r liquid drop radius m; H_g total gas unit mass enthalpy or total heat ; Re Reynolds number; H_s total enthlpy of liquid drop unit mass J/kg; T temperature ${}^oK$; K component ratio; $\vec{u}$ gas speed m/s; K_o decomposition reaction constant 1/s; $\vec{V}$ liquid drop speed m/s; L^* characteristic length m; a surplus oxygen coefficient; m liquid drop mass kg; γ specific heat ratio; M molecular weight kg/gkmol; δ liquid drop

distribution standard deviation; η efficiency; ρ liquid drop mass in unit volume kg/m^3; λ heat conduction coefficient $J/s \cdot m \cdot {}^{o}K$; μ_q gas density kg/m^3; μ viscosity $k \cdot s/m^2$; ρ_l :(illegible) liquid drop density kg/m^3; ν decomposition reaction series; $\vec{f}$ friction force tensor kg/m^3. 62

SUBSCRIPT EXPLANATION

a adiabatic; min minimum; c combustion chamber environment; mix mixture; f fuel; n nth dimension set; F decomposition flame peak; o oxidizer-initial value, basic value; g gas; s liquid drop surface area; i ith root flow tube; t total volume; ing jet injection; th theoretical value; j jth type component; vap vaporization; l liquid drop; exp experimental; max maximum value; cool cool or cold test

I. INTRODUCTION

Following along with the daily development of space flight technology, the requirement for variable thrust liquid fuel rocket engines is becoming more and more pressing. In spacecraft attitude control for such areas as orbital control and planetary and stellar surface probes, variable thrust liquid fuel rocket engine applications, in all cases, are advantageous or indispensible. As far as the wide range of changes in the operating conditions of variable thrust liquid fuel rocket engines is concerned, in terms of energy transfer processes within combustion chambers, they present even higher requirements. Because of this, how to guarantee, within the whole range of thrust changes, the achieving of combustion efficiencies as high as possible and as stable as possible is a research problem wihich possesses practical weapons. In experimental research, one discovers that changes in the operational configuration of variable thrust liquid fuel rocket engines have very great effects on the combustion efficiencies produced. A 5:1 thrust variation ratio liquid fuel rocket engine, within the entire operational flow adjustment range, has changes in combustion efficiency which are

capable of dropping from 90% of design configuration to a low of approximately 60%. We used a 125kg level experimental engine and carried out theoretical and experimental research on the combustion efficiencies in variable thrust operations.

II. THEORETICAL MODELS

As far as the setting up of numerical models of combustion processes within combustion chambers is concerned, using analytic methods in order to describe the interior energy transfer processes of combustion chambers is a problem which people have been probing right along. Since 1946, scores of models have been presented. As far as the utilization of numerical models is concerned, it is possible to understand in relative depth the degree of the effects of changes in the various operational parameters, within combustion chambers, when there are thrust variations, as these changes effect all the various energy transfer processes. As a result of this, one understands control factors and the change configurations for energy transfer during thrust changes and deeply comprehends the causes for changes in combustion efficiency which follow changes in thrust.

We know that energy transfer processes within combustion chambers are composed of a number of complicated subprocesses. Speaking in terms of simple generalization, they mainly accompany the exchange processes associated with high speed chemical reactions in two-phase gas-liquid fields. Jet injection vaporization or atomization processes are relatively complicated. It is difficult to use analytic methods to describe them. At the present time, one is still dependent on experimentation. The speed of gas phase chemical reaction processes is relatively fast. It is not easy to turn them into energy trasfer control processes. Because of this, models take as a condition the complete disintegration of liquid drops in vaporization or atomization. In conjunction with this, it is recognized that gas phase chemical reactions are instantaneous. These models principally describe flow fields aft of jet injection vaporization or atomization zones. In conjunction with this, they lay emphasis on liquid drop evaporation or vaporization diffusion processes.

If one does not consider liquid drop mutual collisions and secondary rupture, as far as liquid drop is concerned, one has the equations set out below for liquid drop quantitative magnitude, mass, momentum, and energy

$$\frac{\partial N_i}{\partial t} + \nabla \cdot (V_i N_i) = 0 \tag{1}$$

$$\frac{\partial \rho_i}{\partial t} + \nabla \cdot (\vec{V}_i \rho_i) = -N_i m_{i,r,l} \tag{2}$$

$$\frac{\partial (\rho_i V_i)}{\partial t} + \nabla \cdot [\rho_i \vec{V}_i \vec{V}_i] = N_i F_i - N_i m_{i,r,l} V_i \tag{3}$$

$$\frac{\partial (\rho_i H_i)}{\partial t} + \nabla \cdot [\rho_i H_i V_i] = N_i Q_i - N_i m_{i,r,l} H_{i,l} \tag{4}$$

In these

$$\rho_i = N_i m_i$$
$$H_i = H_{i,0} + C_{i,l} T_i$$

As far as gases are concerned, it is also possible to set out the equations below for mass, momentum, energy, as well as state

$$\frac{\partial \rho_c}{\partial t} + \nabla \cdot (\rho_g \vec{u}) = \sum_i \sum_j N_i m_{i,r,l}$$
$$\frac{\partial (\rho_g \vec{u})}{\partial t} + \nabla \cdot (\rho_g \vec{u} \vec{u}) = -\nabla p_c + \nabla \cdot (\vec{\tau}) \tag{5}$$

$$- \sum_i \sum_j N_i F_i + \sum_i \sum_j N_i m_{i,r,l} V_i \tag{6}$$

$$\frac{\partial \left\{ \rho_g \left(H_g + \frac{u^2}{2} \right) \right\}}{\partial t} + \nabla \cdot \left[\rho_g \vec{u} \left(H_g + \frac{u^2}{2} \right) \right] = -\nabla \cdot \vec{q}$$
$$+ \nabla \cdot (\vec{u} \vec{\tau}) - \sum_i \sum_j N_i Q_i - \sum_i \sum_j N_i \vec{V}_i F_i$$

$$+ \frac{\partial p_c}{\partial t} + \sum_i \sum_j N_i m_{i,r,l} \left[H_{i,l} + \frac{(V_i)^2}{2} \right] \tag{7}$$

$$\frac{p_c}{\rho_g} = \frac{R}{M_g} T_g \tag{8}$$

If one assumes that flow fields are one dimensional, and, at the same time, only considers stable state processes, not considering the non-homogeneous natures of heat exchange friction, and combustion chamber pressures, one uses localized propellant components in accordance with thermodynamic calculations to determine combustion gas temperature. In this way, equations (1) to (8) described above are capable of being simplified into the equations set out below

$$\frac{dr_j^*}{dx} = \frac{-\dot{m}_{j,\rho,j}^*}{4\pi (r_j^*)^2 \rho_{j,j}^* V_j^*} \tag{9.1}$$

$$\frac{dV_j^*}{dx} = \frac{F_j^*}{\frac{4}{3}\pi (r_j^*)^3 V_j^* \rho_{j,j}^*} \tag{9.2}$$

$$\frac{dT_j^*}{dx} = \frac{Q_j^* - \dot{m}_{j,\rho,j}^* (H_{j,j}^* - H_j^*)}{\frac{4}{3}\pi (r_j^*)^3 \rho_{j,j}^* V_j^* C_{j,j}^*} \tag{9.3}$$

64

$$du = \frac{\sum_i \sum_j N_j^* V_j^* 4\pi \rho_{j,j}^* (r_j^*)^2 dr_j^*}{\sum_i \sum_j \left[N_j^* V_j^* \frac{4}{3} \pi \rho_{j,j}^* (r_j^*)^3 \right]_0} \cdot u_0 \tag{9.4}$$

$$T_g = T_g(K, p_c) \tag{9.5}$$

$$p_c = \rho_g \frac{R}{M_g} T_g \tag{9.6}$$

In these, K is the local component ratio

$$K=\frac{\sum[(V_i\rho_i)_{t_0}-V_i\rho_i]}{\sum[(V_j\rho_j)_{t_0}-V_j\rho_j]} \tag{9.7}$$

u_v is the terminal velocity that hot gases are capable of reaching

$$u_v=\frac{1}{\rho_g}\sum_i\sum_j[N_iV_jm_i]_{t_0}=\frac{\dot{m}}{\rho_g A_c} \tag{9.8}$$

In equation set (9), for the liquid drop gas phase applied force relationship quantity F, one opts for the expression below

$$F=\frac{1}{2}\pi r^2\rho_g C_D|u-V|(u-V)$$

$$C_D=\begin{cases}24R_e^{-1} & R_e\in(0,1)\\ 27R_e^{-0.84} & R_e\in(1,80)\\ 0.271R^{0.217} & R_e\in(80,10^4)\\ 2 & R_e>10^4\end{cases} \tag{10}$$

In this, as far as the liquid drop evaporation or vaporization amount m_{vap} is concerned, considering the heat decomposition reaction, it is determined by the several equilibrium relationships specified below

$$m_{vap}=\frac{4\pi\rho_1 D_1}{AB}\cdot\frac{1}{\frac{1}{r_1}-\frac{1}{r_F}}\cdot\ln\left[\frac{1}{1-BY_{v,s}}\right]$$

$$\frac{4\pi\rho_1 D_1}{B}\cdot\frac{1}{\frac{1}{r_1}-\frac{1}{r_F}}\cdot\ln\left[\frac{1}{1-BY_{v,s}}\right]= \tag{11}$$

$$\frac{4\pi r_F^2}{\sqrt{[C_{p,1}(T_F-T_1)+L_v]^2-C_{p,1}^2(T_F-T_{F,0})^2}}\cdot\frac{RT_F^2}{E}$$

$$\cdot\sqrt{\frac{2K_0\lambda_F Q_C}{T_{F,0}-T_1}}\cdot\left(\frac{P_C M_F}{RT_F}\right)\cdot Y_{v,s}\cdot\exp\left(-\frac{E}{RT_F}\right)$$

(12)

$$T_r = T_{r,\infty} + (T_C - T_{r,\infty}) \exp\left[- \frac{m_r C_{p_1}}{4\pi\lambda_1} \left(\frac{1}{r_\xi} - \frac{1}{r_\infty} \right) \right] \qquad (13)$$

As far as the heat exchange quantity Q is concerned, H_s is related as shown below

$$Q - m_{r,\beta}(H_s - H) = q_r - m_{r,\beta} L_r \qquad (14)$$

In this,

65

$$q_r = \begin{cases} \dfrac{m_1 C_p (T_\beta - T_C)}{e^{\frac{m_r C_p}{4\pi\lambda} \left(\frac{1}{r_1} - \frac{1}{r_2} \right)}_1} & \text{"}f\text{"} \\ \dfrac{m_r C_p (T_C - T_1)}{e^{\frac{m_r C_p}{4\pi\lambda} \left(\frac{1}{r_1} - \frac{1}{r_\infty} \right)}_{-1}} & \text{"}O\text{"} \end{cases}$$

Opting for the use of reasonable boundary conditions and special thermal characteristic calculation methods makes it possible to solve equation set (9) for numerical values. As a result of this, it is possible to solve for and obtain propellant evaporation or vaporization processes along the direction of the axis of the combustion chamber. In conjunction with that, finally, one obtains evaporation or vaporization rates within combustion chambers.

III. EXPERIMENTAL EQUIPMENT AND TEST RESULTS

Fig.1 shows a schematic diagram of the system used for experimental research. The system as a whole is composed of 4 subsystems. From left to right, respectively, are the oxidation agent transport system, the control water supply system, the cooling water control system, and the fuel transport system. Experimental engines opt for the use of coaxial splash or spray ring type jet injector devices. Thrust adjustment is effected through the degree of opening of jet injection paths by which a moveable needle valve simultaneously

adusts two types of propulsion components.

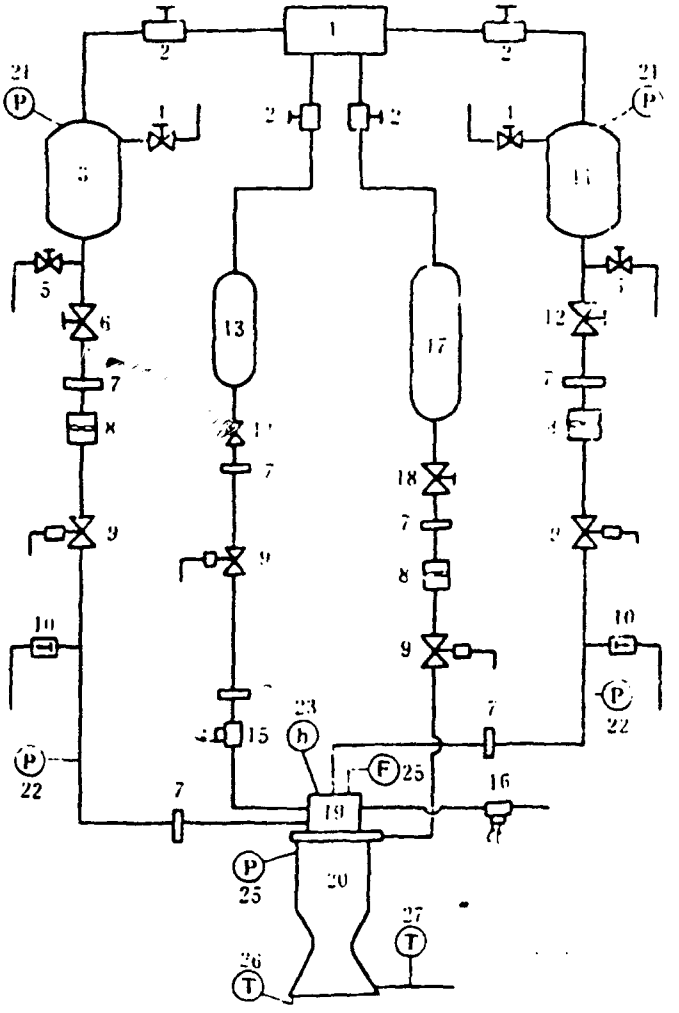

Fig.1 Schematic Diagram of Experimental Engine System

1. 气瓶	2. 减压器	3. 氧化剂贮箱
4. 放气阀	5. 加注/排出阀	6. 氧化剂主阀门
7. 滤网	8. 流量计	9. 气动阀门
10. 吹除阀	11. 燃烧剂贮箱	12. 燃烧剂主阀门
13. 控制水贮箱	14. 控制水主阀门	15. 入口电磁阀
16. 出口电磁阀	17. 冷却水贮箱	18. 冷却水主阀门
19. 喷注器	20. 推力室	

Table 1 Fig.1 Symbol Explanations (1) Gas Source (2) Pressure Reduction Device (3) Oxidizer Storage Tank (4) Gas Release Valve (5) Injection/Exhaust Valve (6) Main Oxidizer Valve (7) Filter Net (8) Flow Meter (9) Pneumatic Valve (10) Blow Off Valve (11) Fuel Storage Tank (12) Main Fuel Valve (13) Control Water Storage Tank (14) Main Control Water Valve (15) Electromagnetic Entry Valve (16) Electromagnetic Exit Valve (17) Cooling Water Storage Tank (18) Main Cooling Water Valve (19) Jet Injector Device (20) Thrust Chamber

① 推进剂	硝酸27/偏二甲肼
② 推力	125～25kg
③ 室压	10～2kg/cm²(绝)
④ 特征长度	0.5～1.0m
⑤ 燃烧室直径	70mm
⑥ 喷管喉径	32mm

Table 2 Main Thrust Chamber Design Parameters (1) propellant: nitric acid 27/nonsymetrical dimethylhydrazine (2) thrust: 125-25kg (3) chamber pressure: 10-2kg/cm^2 (absolute) (4) characteristic length: 0.5-1.0m (5) combustion chamber diameter: 70mm (6) jet tube throat diameter: 32mm

The experimental engine carries out large amounts of heat testing. Fig.2 and Fig.3 show partial results. In the Fig.'s corresponding pressure is $\bar{p}_c = p_c/p_{c,max}$. Fig.2 opts for the use of a water cooled thrust chamber, and one time test results for variable thrust engines with characteristic length $L^* = 0.5$mm. These clearly show engine combustion efficiency $\eta_c{}^*$, a needle valve opening degree of h, and a jet injection pressure drop of $\Delta p_{i,f}$, following along with changes in operational status. Fig.3 is engine variable thrust operation results associated with opting for the use of water cooled thrust chambers, L^*=1.0m.

From operational results, it is possible to see that:

1) in the process of adjusting engine thrust from 25kg-125kg, combustion chamber pressure p_c, jet injection pressure drop Δp_i, and the needle valve degree of opening h all go through broad changes,

2) combustion chamber characteristic speed efficiencies, when adjusted within a range of 25-125kg, show broad changes.

This is particularly obvious in the case of L^*=0.5m combustion

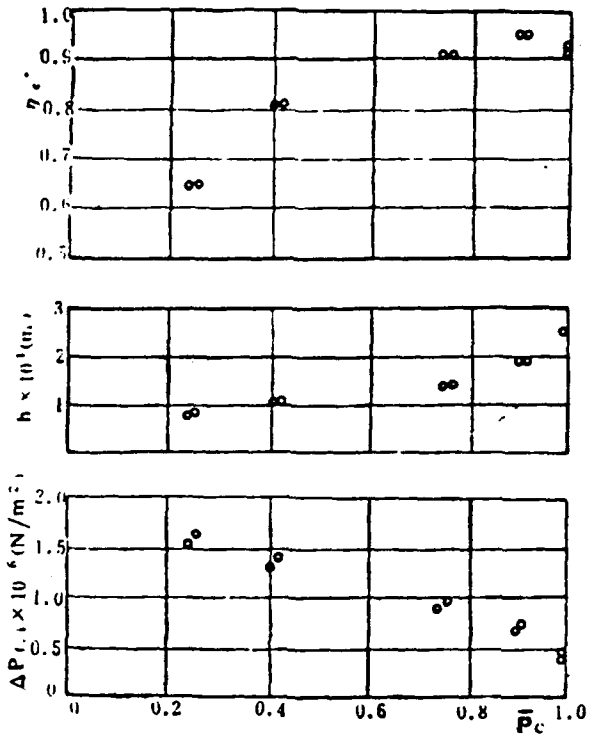

Fig.2 Experimental Results (1), Water Cooled Thrust Chamber, L^* = 0.5m

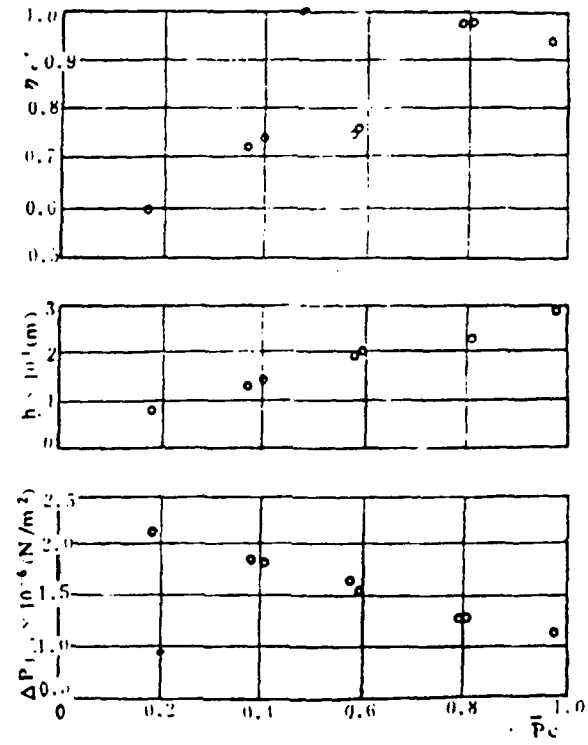

Fig.3 Experimental Results (2), Water Cooled Thrust Chamber L^* = 1.0m

chambers. When $p_c > 0.8$, efficiency η_c^* is capable of reaching over 90%. However, when $p_c < 0.5$, η_c^* drops below 80%. At times of minimum thrust, η_c^* changes are the most abrupt. 67

3) As far as the rules or patterns described above for changes in $\eta_c^* \sim p_c$ are concerned, it goes without saying that they are consistent whether for water cooled thrust chambers or combustion corrosion thrust chambers.

4) When there are changes in combustion chamber characteristic lengths L^*, there is a relatively large effect on $\eta_c^* \sim p_c$ relationship curves. In small operational configurations, this influence is most obvious. For example, when L^* increases from 0.5m to 1.0m, η_c^* values corresponding to small p_c values show relatively large increases.

IV. COMBUSTION EFFICIENCY ANALYSIS

In the general run of liquid fuel rocket engines, due to the majority of jet injection device's being composed of multiple individual jet apertures, aft of the jet injection area, the radial direction mixing is relatively weak. Because of this, it is possible to take the combustion and flows within combustion chambers and divide them into a number of flow tubes parallel to the axis line for purposes of consideration. Each flow tube operates like a little independent combustinon chamber. Because of this the combustion efficiency η_c^* is capable of being expressed as the sum of the effects of the various flow tubes:

$$\eta_c^* = \frac{\sum C_i^*(a_{i,op}) m_{i,op}}{C_{th}^* \dot{m}_t}$$

If one carries out transformations of the equation above, connecting it to the initial jet input component ratio distribution, one then has

$$\eta_c^* = \frac{\sum C_i^*(a_{i,op}) m_{i,op}}{\sum C_i^*(a_{i,mi}) m_{i,mi}} \cdot \frac{\sum C_i^*(a_{i,mi}) m_{i,mi}}{C_{th}^* \cdot \dot{m}_t}$$
$$= \eta_{c,op}^* \cdot \eta_{c,mix}^*$$

From this, we will take combustion efficiency and divide it into two parts. One is $\eta_{c^*,vap}$. It is related to propellant evaporation or vaporization. It is called vaporization efficiency. The second is $\eta_{c^*,mix}$. It is related to propellant mixing. Its name is mixing or mixture efficiency.

1. Mixing Efficiency

From analysis one learns that, in the process of engine thrust variations, the phenomenon of propellant cavitation in tubes will not occur. The "separation" phenomena of jet injector ram atomization or vaporization (that is, RSS phenomena) will also not be severely present. Because of this, in our analysis, we used non-reactive simulation media cold flow tests in order to precisely determine η_{c^*mix}. It will, to a definite degree, reflect actual propellant jet mist mixture configurations. Considering ram atomization processes to be controlled by the geometrical dimensions and momentum of jets, in tests, one opts for the use of similar conditions in which jet injector geometrical dimensions are equal and momentum is equal. As far as flow strength distributions of jet vaporization fields and mixture ratios are concerned, precise measurements were carried out, and, in conjunction with that, mixture efficiencies were calculated out. Fig.4 and Fig.5 show partial experimental results.

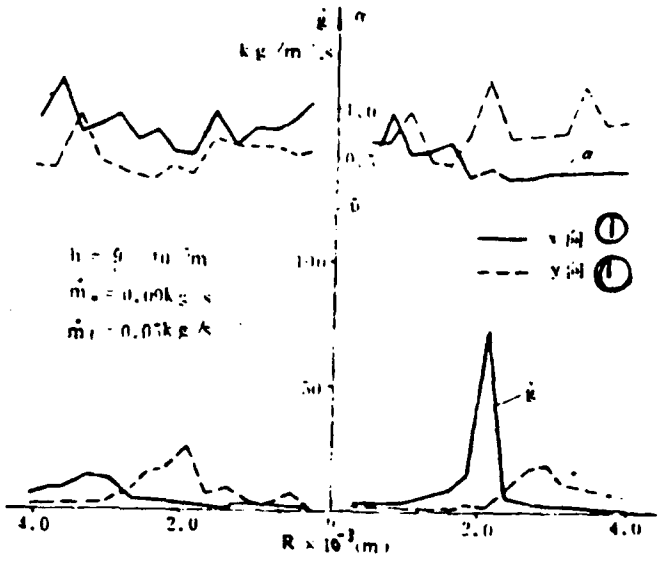

Fig.4 Flow Strength and Mixture Ratio Distributions Under Non-Specified Conditions (1) Direction

Fig.4 shows jet injector flow field and mixture ratio distributions for small thrusts. At this time, because the membrane thickness of jet injection jets is only 0.058mm, as a consequence, the jet injection speed is also very large. Besides this, due to the fact that, with small thrusts, the degree of opening of jet injector devices is very small, the jet display for the smoothness and geometical position tolerances of parts is very sensitive. These factors make jet flow membranes or films very unstable. After the jets come in, they then split up to become thread shaped bundles of liquid even causing jets to show the appearance of clear deflection. As a result of this, the effects of ram mixing between two types of components are weakened and reduced causing flow strength and mixing ratio distributions to be quite uneven . In Fig.4, the displayed flow strength peak values and peak values for mixture ratio distributions are precisely reflections of the effects discussed above. From this, it is clearly demonstrated that the results of propellant mixing, in small operational configurations, are bad.

68

What Fig.5 shows is the status for engine spray flow strength and mixing ratio distributions with specified or rated thrusts. At this time, jet injector jet fluid flims or liquid membranes are relatively thick. Jet injection speed is relatively small. The influence of the processing quality of jet injection devices is correspondingly weak. As a result, jet liquid spray films or membranes are stable. Results for jet injection component fluid films or liquid membranes going through ram and splash or spray mixing are relatively adequate. The broken line obtained from experiments for high operating configurations are also relatively round and smooth.

On the basis of the definitions on the front page, and, making use of cold flow test results, calculations were carried out for mixing efficiencies with variable operational configurations. As to the fact that sampling was not carried out on flow fields as a whole, a choice was made to use the formula below in order to calculate mixing efficiencies:

$$\eta_{C^*,\text{mix},(A)} = \frac{\sum_i g_i C^*(a_i)}{\sum_i g_i C^*(a_{i+1})} \qquad (16)$$

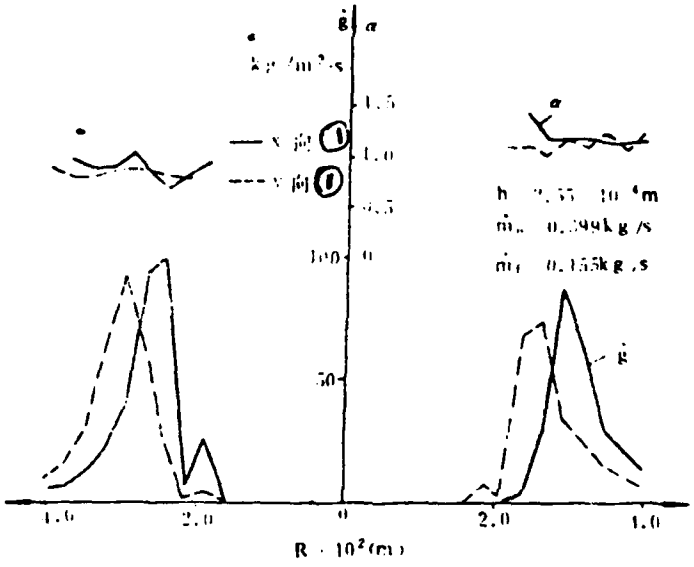

Fig.5 Flow Strength and Mixing Ratio Distributions Under Specified or Rated Conditions (1) Direction

As far as consideration of the structural symmetry of ring shaped jet injector devices which were studied is concerned, in tests, sampling was only done on the radial directions of the four quadrants of jet spray fields. In order to guarantee precision, eacn set of experiments was replicated.

h(mm)	0.255	0.241	0.234	0.151	0.09
p_c(kg/cm^2)	10.0	7.8	5.8	3.8	1.9
$\dot{m}_o$(kg/s)	0.399	0.276	0.258	0.187	0.090
$\dot{m}_f$(kg/s)	0.155	0.147	0.143	0.086	0.050
$\eta_c{}^*{}_{max/A}$	1.007	1.008	1.009	0.959	0.955

Table 3 Mixture Efficiency Calculation Results

Cold test parameters are designed for conditions which simulate a certain hot test condition. Test conditions and corresponding cold test results are set out in Table 3. In the table, the appearance of mixture efficiencies > 1 is due to the fact that $C^*(a_i)$ values are greater than $C^*(a_{inj})$ values, which partially correspond to the surplus oxygen coefficient $a_i > a_{inj}$. These compensate for the partial losses of $a_i < a_{inj}$. At the same time, it is also due to the existance of differences in measurements. From Table 3, it is possible to see that, in a change in operational status or configuration from high to low, the thinner jet injection liquid membranes or fluid films (h) are, the more various types of factors influencing mixing follow this and aggravate things. This leads to a drop in jet device mixture efficiency. Data clearly shows that when $\eta_c > 0.6$, mixing is not perfect, but losses are relatively small. When $\eta_c < 0.6$, mixing is not perfect, and losses gradually increase. The lower the operational configuration is, the smaller the mixing efficiency $\eta_{c^*, mix,th}$ is.

In this, mixing efficiency is completely dependent on the results of cold tests for its calculation. In actual engine operation, due to the existence of combustion reactions, actual mixing states and cold flow tests will show some differences. Moreover, combustion chamber processes, on the basis of flow tube division, will also have definite differences from the actual situation. Because of this, the mixing efficiencies obtained by calculation will not completely match up with the actual situation. However, cold flow tests clearly reflect the important fact that propellant mixtures in combustion chambers follow changes in operational configuration. As a result, they clearly show that the bad turn in mixing processes is an important factor in the lowering of combustion efficiencies under low operational configurations.

69

2. Vaporization Efficiency

As far as evaporation or vaporization efficiencies are concerned, we opted for the use of combustion models which already have vaporization in order to do calculations. It is already known that, in the process of variable thrust operations, as far as changes in the operating conditions for engine jet injectors and combustion chambers are concerned, one sees the occurence of wide changes. Following

operational configuration from high to low, jet injection speed increases continually. Moreover, the degree of opening of jet injector devices decreases continually. These changes necessarily produce effects on the status of vaporized or atomized propellant sprayed into the interior of the combustion chambers.

Detailed analysis of vaporization or misting processes in experimental engines makes it possible to know that mutual collision effects associated with dual component fluid films or liquid membranes occupies a leading position. In reference [4], the liquid drops produced at two mutual collision type jet nozzles are given by

$$D_m \sim \frac{D_f^{0.11} \cdot D_o^{0.33}}{V_f^{0.11} \cdot V_o^{0.33}}$$

From the similarity of atomization processes and control mechanisms, it is possible to recognize in an approximate way that there is, in our experimental engines, the relationship below

$$r_{m,f} = r_{m,o} = A \frac{b_f^{0.11} b_o^{0.33}}{V_f^{0.11} V_o^{0.33}} \qquad (17)$$

In calculations, one opts for the use of equation (17). In the equation, b_f and b_o, respectively, are the thicknesses of propellant liquid membranes or films and oxidizer liquid membranes or films. A, then, is indirectly determined utilizing experimental results for a certain operational configuration. With regard to liquid mist distribution parameters, on the basis of reference [3], for the liquid drop standard deviation δ and spectrum width Z, one picks δ = 0.82 and Z = 3.0.

In evaporization or vaporization efficiency calculation models, initial spray or jet atomization zones are described with simplified models. The key parameters for these areas include jet injection jet disintegration length, L_{sp}, and propellant evaporation or vaporization amount fraction $g_{B(illegible)}$. From the jet mist or vapor status in experimental engines discussed previously and its special features, it is possible to see that, with regard to the

non-uniform characteristics which exist in conical jet atomization fields as well as they themselves, they cause the radial direction exchanges associated with jet injection misting zones in the combustion processes to be relatively strong and violent. As a result, reflux and turbulent flow strengths are all relatively large. This will strengthen the mixing of propellants, and, at the same time, shorten the jet decomposition length. When operational configurations change, changes in combustion chamber conditions will have relatively great effects on jet decomposition lengths. When thrusts go from large to small, jet speeds go from small to large. Under small operational configurations, liquid membrane or fluid film disintegration into liquid threads will cause mutual colllision mixing results between components to vary. At the same time, because chamber pressures drop, this causes combustion gas densities to be reduced. Liquid phase reactions are attenuated, jet injection atomization or misting zone turbulent flow strengths are reduced, and other similar factors. This will make jet decomposition lengths correspondingly longer.

In another area, when one uses natural propellants, the liquid phase reactions must be given consideration. In calculation models, this partial liquid phase reaction is expressed by g_B. From the mechanism of liquid phase reactions, it is possible to know that liquid phase reaction speeds and combustion chamber pressures are related in a direct proportion. At the same time, the level of liquid phase reactions is also in direct proportion with the size of the areas of the liquid phase contact between propellant components. Following along with the alterations in operational configuration described above, all factors are in flux. Because of this, the determined g_B will also change along with the operational configuration. In high operational configurations, high combustion chamber pressures create relatively high liquid phase reaction speeds. At the same time, the numerical values for propellant flow strength are large. Moreover, distributions are relatively concentrated, mixing is relatively perfect, and total contact area between propellants is relatively large. Because of this, in high operational configurations, initial evaporation or vaporization amounts for

propellants are relatively large. Following drops in thrust, initial evaporation or vaporization amounts are reduced. As a first approximation, take L_{sp} and g_B. Following changes in operational configuration, both form linear relationships with chamber pressures p_c, that is,

$$L_{sp}=4.0-0.248(p_c-1.873)$$
$$g_B=0.05+0.0310(p_c-1.873)$$

In these equations, the various constant values are based on the general range of g_B and L_{sp} given in the relevent references. At the same time, consideration is also given to the actual situation of the experimental engine in question as well as consideration being given to the status of burn corrosion on the inner walls after hot tests of combustion corrosion combustion chambers for precise determinations.

Going through the analysis and processing above, it is then possible to carry out calculations for evaporation or vaporization efficiencies. Calculation conditions and mixture efficiency analysis conditions are consistent with each other. Actual conditions and results are set out in Table 4.

From Table 4 it is possible to see that, following along with reductions in thrust, the vaporization efficiency of experimental engines drop.

In the vaporization efficiency calculations discussed above, they are carried out on the basis of one dimensional flow tube theory. No consideration is given to the effects of non-uniform spray area propellant distributions on evaporation or vaporization efficiencies. This influence, under low operational configurations, will not be negligible. Because of this, the evaporation or vaporization efficiencies obtained by calculation follow changes in operational configuration and show a certain disparity with the actual situation. However, in terms of mechanism, they illucidate the trends in evaporation or vaporization efficiencies as they follow changes in operational configuration. They clearly show that, when under low operational configurations, L^*=0.5m engines have relatively large effects due to imperfect evaporation or vaporization lowering combustion efficiencies.

p_c(kg/cm²)	1.873	3.843	5.873	7.983	9.933
h(mm)	0.0922	0.1545	0.2321	0.2440	0.2570
$V_{o,th}$(m/s)	48.81	45.59	42.59	39.93	35.86
$V_{f,th}$(m/s)	29.16	26.57	24.66	22.93	21.37
V(m/s)	35.1	32.8	30.48	28.63	26.71
$r_{m,s}$(um)	107.3	131.9	161.0	175.1	195.0
L_{sp}(cm)	4.0	3.51	3.00	2.49	2.00
g_s	0.05	0.111	0.174	0.240	0.300
η_c^*,vap,th	0.710	0.768	0.761	0.807	0.860

Table 4 Evaporation or Vaporization Efficiency Calculation Results

3. Comprehensive Analysis of Characteristic Speed Efficiency

On the foundation of solutions for η_c^*,mix,th and η_c^*,vap,th obtained in cold flow tests and theoretical calculations, from η_c^*,th = η_c^*,mix,th '(illegible) η_c^*,vap,t, it is possible to obtain the characteristic speed efficiency of theoretical analysis η_c^*,th. In Fig.6, one takes changes in the theoretical values η_c^*,th and the test values η_c^*,exp and makes a comparison. In the Fig., $\bar{\eta}_{c^*} = \eta_{c^*}/\eta_{c^*,max}$.

From Fig.6 it is possible to see that η_c^*,th and η_c^*,exp are consistent in the overall rules or patterns they obey in following changes in operational configuration. Proceeding to the next step, this explains this article's being directed at the analytical models discussed above which were set up for variable thrust rocket engines. In terms of mechanisms, they reflect factors influencing combustion processes inside actual engines.

In Fig.6, one sees reflected the fact that η_c^*,th and η_c^*,exp have associated with them patterns or rules in their changes which, in terms of actual trends, still show the existence of differences. The reasons are: 1) when calculating η_c^*,vap,th, there is no consideration given to the influence of non-uniform mixing

distributions in spray zones. This influence, during low operational

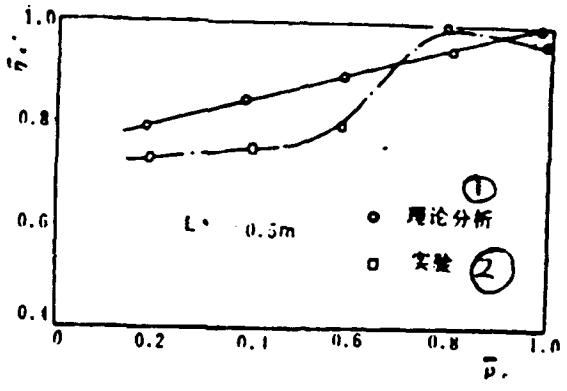

Fig.6 Comparison of $\eta_{c'}^{*}$ Values from Theoretical Analysis and Experimentation (1) Theoretical Analysis (2) Experimentation

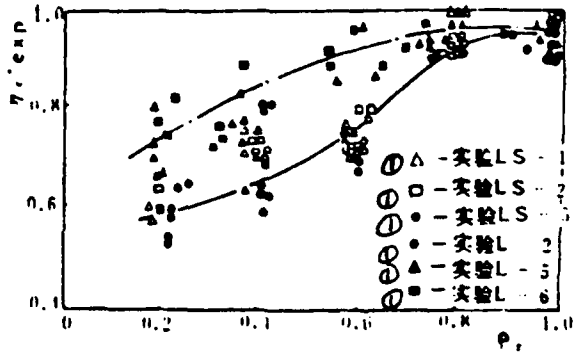

Fig.7 A Comparison of Efficiencies with Different Combustion Chamber Lengths (I) Solid Symbol L^{*} =1.0m Hollow Symbol L^{*} =0.5m (1) Test

configurations, is particularly obvious. 2) When calculating $\eta_{c^{*}vap,th}^{*}$, assume that the gas phase chemical reactions are completed instantaneously, and they do not produce effects on combustion

efficiencies. Moreover, when actual chamber pressures are relatively low, chemical reaction speeds will drop. Actual combustion gas temperatures will be lower than equilibrium temperatures. As a result of this, effects will be produced on evaporation or vaporization speed. 3) η_{c}*mix,th is obtained based on cold flow experimentation. It shows certain discrepancies with actual hot test states. 4) Under various operational configurations, actual measurements of liquid jet sprays were not carried out. Generalized applications were made of the test results of previous people. It is difficult to precisely reflect the actual rules or patterns for the jet injector devices in question. 5) In calculations, we ignored heat transmission and friction losses.

In order to carry a step further checks on the level of influence on energy transfer efficiencies of evaporation or vaporization and mixing when testing engines under varied operational configurations, one opts for the use of different lengths of combustion chamber to carry out hot tests. Experimental results are shown in Fig.7. When L^* increases from 0.5m to 1.0m, there are relatively large increases in combustion efficiencies under low operational configurations. We acknowledge that alterations in characteristic length are key influences on the degree of perfection of evaporation or vaporization of propellants. From results, one infers that, as far as L^*=0.5m variable thrust engines are concerned, following along with reductions in thrust, the evaporation or vaporization efficiency is correspondingly diminished. This is in line with the results of the previous theoretical analysis. 71

Fig.8 gives η_{c}*,exp values for L^*=0.8m and L^*=1.0m. From the comparison in the Fig., it is possible to see that the effects on η_{c}*,exp are not obvious when L^* rises from 0.8m to 1.0m. Comparing the obvious effects on η_{c}*,exp with L^* increased from 0.5m to 1.0m, and, at the same time, considering the direct responsivness of η_{c}*vap to L^*, we recognize that, speaking in terms of the actual engine in question, when L^*=1.0m, η_{c}*,vap already tends toward a saturated value. The significance of this is that propellant evaporation or vaporization, as far as the various

operational configurations are concerned, is already basically complete. It is no longer a key factor influencing efficiency $\eta_{c^*,exp}$. Because of this, L^*=1.0m's η_{c^*exp}, in reality, reflects the magnitudes of other energy losses besides mixing efficiency and evaporation or vaporization losses.

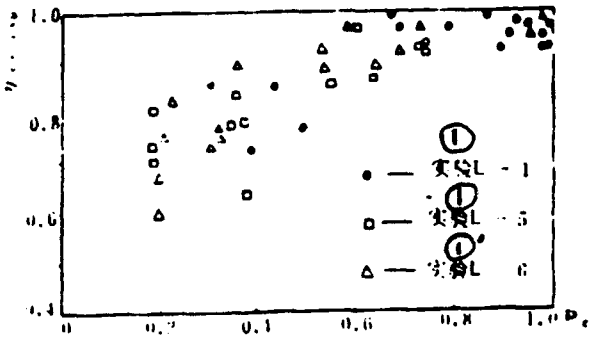

Fig.8 A Comparison of Efficiencies With Different Combustion Chamber Lengths (II) Solid Symbol L 0.8m Hollow Symbol L =1.0m (1) Test

Fig.9 gives actual characteristic speed efficiencies $\eta_{c^*,exp}$ with L^*=1.0m and the cold or cool flow test results ($\eta_{c^*,mix}$)cool for the same jet injection device. As was discussed before, when L^*=1.0m, $\eta_{c^*,vap} \approx 1.0$. Because of this, ($\eta_{c^*,exp}$)$L^*$=1.0 = $\eta_{c^*,mix,exp}$. Comparing ($\eta_{c^*,mix}$)cool and ($\eta_{c^*,exp}$)$l^* < 1.0$m, it is possible to know that the difference in values between them follows drops in operational configuration and increases. Under low operational configurations, hot test results ($\eta_{c^*,exp}$)l=1.0m, compared to cold or cool test results $\eta_{c^*mix,cool}$, will be much lower. The explanation for this is that cold flow test results are still not adequate to reflect the actual mixing processes of the engine in question. At the same time, this reminds people that, under low operational configurations, there is the possibility of the existence of other control factors related to energy transfers. From observations during engine hot tests, following along with changes in operational configurations, there are clear differences with the state of expelled combustion gases in jet tubes. Under high operational configurations, the combustion gases expelled are red and bright. However, under low operational configurations, the flame brightness is extremely low. Using thermocouples to measure, stagnent temperatures were approximately 1400°K. This will be much lower

than the chemical thermodynamic equilibrium temperature for calculation, 2700°K, as compared with corresponding conditions. We know that there is a close relationship between the speeds at which chemical reactions are carried out and temperatures and pressures. When combustion chamber pressures are very low, the non-equilibrium factors associated with the chemical reactions then have the possibility of becoming one of the control factors associated with energy transfers.

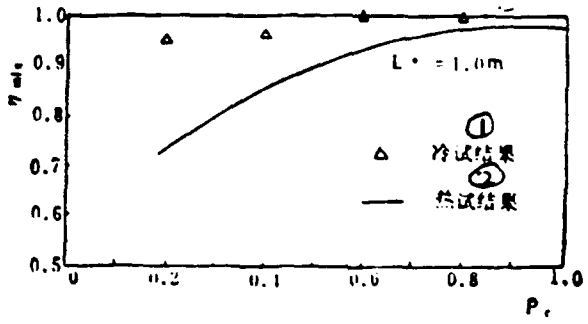

Fig.9 A Comparison of Mixture Efficiencies in Cool and Hot Tests (1) Cold or Cool Test Results (2) Hot Test Results

V. CONCLUSIONS

1. As far as variable thrust liquid rocket motors are concerned, following along with alterations in operational configuration, the combustion efficiencies will show the occurence of changes. With regard to the actual L^*=0.5m engine, when the thrust is adjusted down in a 5:1 alteration, theory and experimentation prove that the degree of imperfection or incompleteness of evaporation (vaporization) and mixing follow reductions in thrust and increase. Tests also verify that appropriate increases in the length L^* are capable of causing combustion efficiencies under low operational configurations to exhibit relatively wide increases. For example, an engine with thrust that changes from 125kg to 25kg, will have L^* rise from 0.5m

72

to 0.8m, causing combustion efficiency to follow the range of the change in thrust and be reduced from 95%-60% to 95%-75%. Moreover, the increase in engine weight will not exceed 5%.

2. Research clearly shows that the key factors in making propellant mixing processes imperfect or incomplete are increases in jet injector flow speeds during injector flow adjustment processes and reductions in the thickness of liquid membranes or fluid films. Making fluid films or liquid membranes unstable, they disintegrate to become strip shaped bundles of liquid, causing deviations in ram mixing results. Because of this, in designs, it is necessary to make delicately balanced selections for the jet injector degrees of opening h_{max} and h_{mix} within the flow adjustment range. An ideal variable thrust liquid rocket motor or engine will execute simultaneous control of propellant component ratios and jet injection speeds.

3. When nitric acid 27/asymmetrical dimethyl hydrazine propellants are used in variable thrust liquid rocket engines, at very low pressures, the speeds of chemical reactions drop, which is worthy of serious attention. It has the possibility of becoming one among the control factors for energy transfer.

REFERENCES

[1] Poewll, W.B.; "Simplified Procedures for Correlation of Experimentally Measured and Predicted Thrust Chamber Performance", NASA, TM 33-548, 1973,1.

[2] Sternfeld, Han J.; "Energy Losses in High Performance Rocket Engines Under Conditions of Varied Thrust", Trans. Chen Qizhi, National Defense Science and Technology University, 1982

[3] Buschulte, W; "Studies on Energy Transfer Associated with Liquid Fuel Rocket Engine Thrust Adjustments"; Trans. Chen Qizhi, National Defense Science and Technology Univeristy, 1981.9

[4] Chen Qizhi (ed.); "Variable Thrust Liquid Rocket Engine Thrust Chamber Energy Transfers"; National Defense Science and Technology University, 1982.8

[5] Sutton, R.D.; "Propellant Spray Combustion Processes During Stable and Unstable Liquid Rocket Combustion", AD-722473.

[6] Priem, Richard J. and Heidman, Marcus F.; "Propellant Vaporization as a Design Criterion for Rocket Engine Combustion Chambers", NASA TR-R67, 1960.

[7] Knight, R.M., Nurick, W.H.; "Correlation of Spray Dropsize Distribution and Injector Variables", NASA, CR-]074]], 1969. 9.

[8] Tong Jingshan, Li Jing; Calculations of the Thermophysical Properties of Fluids; Qinghua University Press, 1982

[9] Zhuang Fengchen, Liu Xiaodi; "Calculation Model for High Pressure Equilibrium Evaporation or Vaporization Associated With Spontaneously Combustive Propellant Component Liquid Drops"; National Defense Science and Technology University Journal, 1983.8

DISTRIBUTION LIST

DISTRIBUTION DIRECT TO RECIPIENT

ORGANIZATION	MICROFICHE
B085 DIA/RTS-2FI	1
C509 BALL0C509 BALLISTIC RES LAB	1
C510 R&T LABS/AVEADCOM	1
C513 ARRADCOM	1
C535 AVRADCOM/TSARCOM	1
C539 TRASANA	1
Q592 FSTC	4
Q619 MSIC REDSTONE	1
Q008 NTIC	1
Q043 AFMIC-IS	1
E051 HQ USAF/INET	1
E404 AEDC/DOF	1
E408 AFWL	1
E410 ASDTC/IN	1
E411 ASD/FTD/TTIA	1
E429 SD/IND	1
P005 DOE/ISA/DDI	1
P050 CIA/OCR/ADD/SD	2
1051 AFIT/LDE	1
CCV	1
P090 NSA/CDB	1
2206 FSL	1

Microfiche Nbr: FTD91C000756
FTD-ID(RS)T-0571-91